A Floe Size Dependent Scattering Model in Two- and Three-dimensions for Wave Attenuation by Ice Floes

Michael H. Meylan[1]

[1]School of Mathematical and Physical Sciences, The University of Newcastle, Callaghan, NSW 2308, Australia

Christopher Horvat[2]

[2]Institute at Brown for Environment and Society, Brown University, Providence, RI, USA

Cecilia M. Bitz[3]

[3]Department of Atmospheric Sciences, University of Washington, Seattle, WA, USA

Luke G. Bennetts[4]

[4]School of Mathematical Sciences, University of Adelaide, Adelaide, SA 5005, Australia

Abstract

Two- and three-dimensional models are proposed for ocean-wave attenuation due to scattering by ice floes in the marginal ice zone, in which the attenuation rate depends on the horizontal size of the individual floes. The scattering models are shown to reproduce the behaviour of wave attenuation over short wave periods. However, it is shown that scattering alone cannot explain the observed asymptotic dependence of attenuation at long wave periods. Based on these findings, it is proposed that attenuation models consist of a scattering component supplemented by an empirical damping term based on measurements, so that attenuation over all periods is correctly modelled. Computer code to calculate wave attenuation through a field of ice floes is provided in the supplementary material.

1 Introduction

Understanding the interaction between ocean waves and the sea-ice covered ocean has applications ranging from predicting sea ice extent to safe navigation. Ocean waves are frequently observed to impact the sea ice cover and to be attenuated by the ice cover (Kohout et al., 2014; Meylan et al., 2014). There is evidence that ocean waves modulate sea-ice extent (Zhang et al., 2016; Bennetts et al., 2017; Boutin et al., 2018; Roach et al., 2018, 2019; Bateson et al., 2020), and that attenuation of waves by sea ice protects ice shelves (Massom et al., 2018; Chen et al., 2019b).

A concerted effort has emerged to include and evolve the coupled representation of sea ice and ocean surface waves into large-scale models for improved ice–ocean physics and prediction (Bateson et al., 2020; Boutin et al., 2020; Roach et al., 2019; Dumont et al., 2011; Williams et al., 2013a,b; Horvat and Tziperman, 2015; Horvat et al., 2016; Williams et al., 2017; Meylan et al., 2020). This effort has been focused mainly in the marginal ice zone (MIZ), where sea ice is highly fragmented, mobile, and in contact with ocean waves. Models include a parameterisation of the wave attenuation coefficient (i.e. the exponential rate of wave attenuation over distance travelled), generically written $\alpha(A, T, h, a)$, where A is the wave amplitude, T is wave period, h is sea ice thickness, and a is the floe radius.

Measurements of wave attenuation by sea ice began with pioneering work by members of the Scott Polar Institute (Squire and Moore, 1980; Wadhams et al., 1988). In recent years, technological developments have allowed more detailed measurements of wave attenuation (Kohout et al., 2014;

Meylan et al., 2014; Doble et al., 2015; Rogers et al., 2016; Cheng et al., 2017; Meylan et al., 2018; Sutherland et al., 2018; Thomson et al., 2018; Rabault et al., 2020; Horvat et al., 2020; Rogers et al., 2020; Alberello et al., 2020) and better constraints on the form of α. The data collected show the attenuation coefficient for long-period waves (above 10 seconds) is approximately proportional to the wave period to the power of minus two, i.e. $\alpha \sim T^{-2}$ for $T > 10\,\mathrm{s}$.

Theoretical modelling of wave attenuation by sea ice has been the subject of parallel research advances (Squire, 2020). Models can be broadly divided into two categories: those treating sea ice as a viscous layer (Weber, 1987; Keller, 1998; Wang and Shen, 2010a; Sutherland et al., 2019; Chen et al., 2019a; Cheng et al., 2020) and those treating it as a scattering medium (Meylan et al., 1997; Kohout and Meylan, 2009; Bennetts et al., 2010; Bennetts and Squire, 2012; Montiel et al., 2016). Viscous layer models idealise the field of floes in the MIZ as a continuum, and are intuitively applicable in the long-wavelength limit. The layer models have been extended beyond viscosity, for example, Voermans et al. (2019) considered attenuation due to turbulence. In contrast, scattering models involve a large collection of individual floes, where the standard model for wave scattering by a single floe is based on a floating elastic thin plate model, and accounts for the compliant bending of large floes while preserving the rigidity of small floes (Meylan and Squire, 1994; Meylan, 2002; Bennetts and Williams, 2010).

With the exception of Perrie and Hu (1996) and the recent work Meylan et al. (2020), only two-dimensional (one horizontal dimension and one depth dimension) scattering models that have been implemented in large-scale prediction models, and often assuming floe lengths are much larger than the wavelength to avoid artificial resonance effects (Kohout and Meylan, 2008; Williams et al., 2013a; Bennetts and Squire, 2012). Contemporary three-dimensional scattering models of wave attenuation (Peter and Meylan, 2009; Bennetts and Squire, 2009; Bennetts et al., 2010; Montiel et al., 2016) have not yet produced a formula for α suitable for inclusion in large-scale models, and this is the subject of ongoing research (Meylan and Bennetts, 2018).

Scattering of ocean waves by ice floes only occurs when there is a momentum exchange between the ice floe and ocean waves. In turn, the momentum exchange implies that a force is applied to the ice floe, and hence it is liable to fracture. Therefore, the effect of scattering is central to understanding ice pack break up due to waves and other processes (Kohout et al., 2016; Herman et al., 2018). After the ice pack has been broken into smaller floes, scattering is likely to have a weaker effect, especially for the long–period waves which persist far into the MIZ (Collins et al., 2015; Dolatshah et al., 2018).

There is clear evidence from experiments that the ice cover causes energy to be removed from waves at a much greater rate than for an ocean without an ice cover. However, there is no evidence to show what the mechanism is that removes this energy. There is evidence to suggest that it is caused by under-ice friction (Liu and Mollo-Christensen, 1988; Ardhuin et al., 2016; Boutin et al., 2018), floe collisions (Shen and Squire, 1998; Bennetts and Williams, 2015; Yiew et al., 2017), overwash (Toffoli et al., 2015; Nelli et al., 2017, 2020), or viscoelastic bending (Wang and Shen, 2010b; Mosig et al., 2015). There is also evidence that the wave action breaks the floes in a highly active breaking region (which scattering is probably dominant) until the floes are sufficiently fractured that scattering is negligible and other mechanisms then dominate the wave attenuation (Ardhuin et al., 2020). Further evidence of this can be recent results on floe breaking (Voermans et al., 2019).

Despite the need to model wave attenuation and sea ice fracture accurately, a model including all required features of attenuation is lacking. This paper proposes an open-source model that captures both the short and long-period wave attenuation through the sea-ice cover. For short periods, we use scattering theory to account for the strong attenuation of small floes, including the effect of floe size variability. For long periods we propose an extra term which is based on experimental measurements which can easily be updated with additional experimental data or appropriate theory. The computer code required to run the model is provided as supplementary material.

2 Attenuation, scattering and dissipation

There is some ambiguity in the terms attenuation, scattering and dissipation and we want to be clear here what we mean by these words. Attenuation is the observed decrease in wave height as it propagates through the MIZ. Scattering is the process that changes the direction of propagation without removing energy and dissipation is a process which removes wave energy. Both scattering and dissipation can lead to attenuation.

A critical difference between scattering and dissipation is that scattering will lead to broadening of the wave direction and eventually to an isotropic wave field (if there is no significant dissipation). This is attested to in models (Montiel et al., 2016), although there is no clear observational evidence. Scattering must involve momentum exchange and hence high forces and is likely to cause fracture or melting. Scattering models have clear and straightforward physics, which is the basis for offshore engineering and ship design and which has been well validated in laboratory experiments (Meylan et al., 2015; Montiel et al., 2013a). It is possible that scattering only plays a significant role in the active breaking region, but we believe its influence is more comprehensive than this. However, we acknowledge that evidence to prove this is lacking.

3 Wave scattering by individual ice floes

The scattering model treats an ice floe as a floating, elastic plate, which behaves as a rigid body in the case of long waves or large thickness. We present a simple numerical method that works in two- and three-dimensions to high accuracy and efficiency based on eigenfunction matching. The solution in three-dimensions was first given by Peter et al. (2004), and the solution in two-dimensions was first given by Fox and Squire (1994) for the semi-infinite case. Floating elastic plates have been the subject of laboratory experiments to validate and show limitations of the model in terms of the plate motion (Montiel et al., 2013a,b; Meylan et al., 2015; Yiew et al., 2016) and of the scattered wave field (Bennetts et al., 2015; Nelli et al., 2017; Sree et al., 2017). While the solution to our problem has appeared previously, the simplified numerical solution in two–dimensions given below, which is based on symmetry, has not appeared previously to our knowledge. We give detailed descriptions to help to understand the computer code which accompanies the paper.

We begin by stating the governing equations for the floe–water system. We assume that the floe has a uniform thickness of h, the seafloor is flat, and that all motions are time-harmonic with radian frequency ω. The velocity potential in the water, Φ, can be expressed as,

$$\Phi(\mathbf{x}, z, t) = \mathrm{Re}\left\{\phi(\mathbf{x}, z)\mathrm{e}^{-\mathrm{i}\omega t}\right\}, \tag{1}$$

where the reduced velocity potential ϕ is complex-valued, and $\mathbf{x}$ is the horizontal spatial variable, such that $\mathbf{x} = x$ in two-dimensions and $\mathbf{x} = (x, y)$ in three-dimensions, and z is the depth variable, which points upwards, with the water surface at $z = 0$ and the seafloor at $z = -H$. The ice floe is on the free surface ($z = 0$) and occupies the domain Ω, where

$$\Omega = \{\mathbf{x} : |\mathbf{x}| \leq a\}, \tag{2}$$

a is the ice floe radius (strictly, in two-dimensions $2\,a$ is the ice floe length).

The reduced potential satisfies the boundary value problem

$$\Delta\phi + \partial_z^2\phi = 0, \quad -H < z < 0, \tag{3a}$$

$$\partial_z\phi = 0, \quad z = -H, \tag{3b}$$

$$\partial_z\phi = K\,\phi, \quad z = 0, \quad \mathbf{x} \notin \Omega, \tag{3c}$$

$$(F\Delta^2 + 1 - K\,\gamma)\partial_z\phi = K\,\phi, \quad z = 0, \quad \mathbf{x} \in \Omega, \tag{3d}$$

where Δ is the Laplacian operator in the horizontal plane. The constant $K = \omega^2/g$ is the (deep water) wavenumber, in which $g \approx 9.81\,\mathrm{m\,s^{-2}}$ is the constant of gravitational acceleration. The parameters F and γ are non-dimensional versions of the flexural rigidity and mass of the floe, respectively,

$$F = \frac{Y\,h^3}{12\,(1-\nu^2)\,\rho\,g} \quad \text{and} \quad \gamma = \frac{\rho_i\,h}{\rho}, \tag{3e}$$

where $\rho \approx 1025\,\mathrm{kg\,m^{-3}}$ is the water density, $Y \approx 6\,\mathrm{GPa}$ is the Young's modulus of sea ice, $\nu \approx 0.3$ is its Poisson's ratio, and $\rho_i \approx 925.5\,\mathrm{kg\,m^{-3}}$ is its density (Timco and Weeks, 2010).

The floe edges are assumed free, so that the bending moment and shear stress vanish. In the two-dimensional problem, the free-edge conditions are

$$\partial_x^2\partial_z\phi = 0, \quad z = 0, \quad |\mathbf{x}| = a, \tag{3f}$$

$$\partial_x^3\partial_z\phi = 0, \quad z = 0, \quad |\mathbf{x}| = a. \tag{3g}$$

In three-dimensions, they are

$$\left\{\Delta - (1-\nu)r^{-1}\left(\partial_r + r^{-1}\partial_\theta^2\right)\right\}\partial_z\phi = 0, \quad z = 0, \quad |\mathbf{x}| = a, \tag{3h}$$

$$\left\{\partial_r\Delta - (1-\nu)r^{-2}\left(\partial_r + r^{-1}\right)\partial_\theta^2\right\}\partial_z\phi = 0, \quad z = 0, \quad |\mathbf{x}| = a, \tag{3i}$$

where (r, θ) are polar coordinates, such that

$$x = r\cos\theta \quad \text{and} \quad y = r\sin\theta. \tag{4}$$

The vertical eigenfunctions for (3) are

$$\phi_m(z) = \frac{\cos k_m(z+H)}{\cos k_m H}, \quad m = 0, 1, \ldots, \quad \mathbf{x} \notin \Omega \tag{5a}$$

$$\text{and} \quad \psi_m(z) = \frac{\cos \kappa_m(z+H)}{\cos \kappa_m H}, \quad m = -2, -1, \ldots, \quad \mathbf{x} \in \Omega. \tag{5b}$$

The wavenumbers involved in (5) are $k = k_m$ $(m = 0, 1, \ldots)$, where

$$k\tan(kH) = -K, \tag{6}$$

and $\kappa = \kappa_m$ $(m = -2, -1, \ldots)$, where

$$\kappa\tan(\kappa H) = \frac{-K}{F\kappa^4 + 1 - K\gamma}. \tag{7}$$

We let $k_0, \kappa_0 \in \mathrm{i}\mathbb{R}_-$, $k_m, \kappa_m \in \mathbb{R}_+$ $(m = 1, 2, \ldots)$, such that $k_1 < k_2 < \ldots$ and $\kappa_1 < \kappa_2 < \ldots$, and $\kappa_{-2}, \kappa_{-1} \in \mathbb{C}$, such that $\kappa_{-1} = -\overline{\kappa_{-2}}$ (in general; for details see Bennetts et al., 2007).

We note that

$$\int_{-H}^{0} \phi_m(z)\phi_n(z)\,\mathrm{d}z = A_m\delta_{mn}, \tag{8}$$

where

$$A_m = \frac{1}{2}\left(\frac{\cos k_m H \sin k_m H + k_m H}{k_m \cos^2 k_m H}\right), \tag{9}$$

and

$$\int_{-H}^{0} \phi_n(z)\psi_m(z)\,\mathrm{d}z = B_{mn}, \tag{10}$$

where

$$B_{mn} = \frac{k_n \sin k_n H \cos \kappa_m H - \kappa_m \cos k_n H \sin \kappa_m H}{(\cos k_n H \cos \kappa_m H)\,(k_n^2 - \kappa_m^2)}. \tag{11}$$

Radiation conditions are applied to ensure unique solutions to governing equations (3). In two-dimensions, the radiation conditions are

$$\phi(\mathbf{x}, z) \sim \begin{cases} \phi_I(\mathbf{x}, z) + \mathcal{R}\phi_I(-\mathbf{x}, z) & x \to -\infty, \\ \\ \mathcal{T}\phi_I(\mathbf{x}, z) & x \to \infty, \end{cases} \tag{12}$$

where $\phi_I(x, z)$ is the incident wave potential

$$\phi_I(\mathbf{x}, z) = \mathrm{e}^{\mathrm{i}kx}\phi_0(z), \tag{13}$$

in which $k = \mathrm{i}k_0$ is the incident wavenumber, and $\mathcal{R}$ and $\mathcal{T}$ are the reflection and transmission coefficients, respectively. In three-dimensions, the radiation condition is

$$\sqrt{r}\,(\partial_r - \mathrm{i}k)\,(\phi - \phi_I) \to 0 \quad \text{as} \quad r \to \infty. \tag{14}$$

3.1 Solution for two-dimensional model

We solve the two-dimensional problem by writing the solution as the sum of a symmetric (even) solution, $\phi^{(s)}(x, z) = \phi^{(s)}(-x, z)$, and an anti-symmetric (odd) solution, $\phi^{(a)}(x, z) = -\phi^{(a)}(-x, z)$, which can be solved on $x \in (-\infty, 0)$. This splitting, simplifies the solution to the finite problem and makes it a trivial extension of the semi-infinite solution of Fox and Squire (1994). To the best of the authors' knowledge, this idea has not appeared in the literature previously.

Without loss of generality, we assume that the incident potential has unit amplitude, and the symmetric solution is given by

$$\phi^{(s)}(x, z) = \phi_I(x, z) + \sum_{m=0}^{M} a_m^{(s)} e^{k_m(x+a)}\phi_m(z), \ x < -a, \tag{15}$$

in the open water, and

$$\phi^{(s)}(x, z) = \sum_{m=-2}^{M} b_m^{(s)} \frac{\cosh(\kappa_m x)}{\cosh(\kappa_m a)}\psi_m(z), \ -a \le x \le 0, \tag{16}$$

in the ice covered water, for some suitably large M. To solve for the coefficients $a_m^{(s)}$ $(m = 0, \ldots, M)$ and $b_m^{(s)}$ $(m = -2, \ldots, M)$, we use continuity of pressure and horizontal velocity to equate the potential and its derivative at $x = -a$, which gives, respectively,

$$\phi_0(z) + \sum_{m=0}^{M} a_m^{(s)}\phi_m(z) = \sum_{m=-2}^{M} b_m^{(s)}\psi_m(z), \tag{17}$$

and

$$-k_0\phi_0\left(z\right)+\sum_{m=0}^{M}a_m^{(s)}k_m\phi_m\left(z\right)=-\sum_{m=-2}^{M}b_m^{(s)}\kappa_m\tanh(\kappa_m h)\psi_m(z). \tag{18}$$

Multiplying both equations by $\phi_l(z)$ $(l=0,\ldots,M)$ and integrating over $z\in(-H,0)$, we obtain the system

$$\mathrm{e}^{-\mathrm{i}ka}A_0\delta_{0l}+a_l^{(s)}A_l=\sum_{m=-2}^{M}b_m^{(s)}B_{ml}, \tag{19a}$$

$$\text{and}\quad -k_0\mathrm{e}^{-\mathrm{i}ka}A_0\delta_{0l}+a_l^{(s)}k_lA_l=-\sum_{m=-2}^{M}b_m^{(s)}\kappa_m\tanh(\kappa_m a)B_{ml}, \tag{19b}$$

for $l=0,1,\ldots,M$. Applying the free-edge conditions (3e–f) closes the system with the equations

$$-\sum_{m=-2}^{M}b_m^{(s)}\kappa_m^3\tan\kappa_m h=0, \tag{19c}$$

$$\text{and}\quad \sum_{m=-2}^{M}b_m^{(s)}\kappa_m^4\tanh(\kappa_m a)\tan\kappa_m h=0. \tag{19d}$$

The system (19) is solved for the coefficients $a_m^{(a)}$ $(m=0,\ldots,M)$ and $b_m^{(a)}$ $(m=-2,\ldots,M)$.

The anti-symmetric solution is found in an almost identical manner. We express the solution as

$$\phi^{(a)}(x,z)=\phi_I(x,z)+\sum_{m=0}^{M}a_m^{(a)}e^{k_m(x+a)}\phi_m(z),\quad x<-a, \tag{20}$$

and

$$\phi^{(a)}(x,z)=\sum_{m=-2}^{M}b_m^{(a)}\frac{\sinh(\kappa_m x)}{\sinh(-\kappa_m a)}\psi_m(z),\quad -a\le x\le 0. \tag{21}$$

Applying continuities leads to

$$\mathrm{e}^{-\mathrm{i}ka}A_0\delta_{0l}+a_l^{(a)}A_l=\sum_{m=-2}^{M}b_m^{(a)}B_{ml}, \tag{22a}$$

$$\text{and}\quad -\hat{k_0}\mathrm{e}^{-\mathrm{i}ka}A_0\delta_{0l}+a_l^{(a)}k_lA_l=-\sum_{m=-2}^{M}b_m^{(a)}\kappa_m\coth(\kappa_m a)B_{ml}, \tag{22b}$$

for $l=0,1,\ldots,M$, and the free-edge conditions give

$$-\sum_{m=-2}^{M}b_m^{(a)}\kappa_m^3\tan\kappa_m h=0, \tag{22c}$$

$$\text{and}\quad \sum_{m=-2}^{M}b_m^{(a)}\kappa_m^4\coth(\kappa_m a)\tan\kappa_m h=0. \tag{22d}$$

The total potential is

$$\phi(x,z) = \frac{1}{2}\left(\phi^{(s)}(x,z) + \phi^{(a)}(x,z)\right), \tag{23}$$

and the reflection and transmission coefficients are (from adding the symmetric and anti-symmetric solutions), respectively,

$$\mathcal{R} = \frac{\mathrm{e}^{\mathrm{i}ka}}{2}\left(a_0^{(s)} + a_0^{(a)}\right) \tag{24a}$$

$$\text{and} \quad \mathcal{T} = \frac{\mathrm{e}^{\mathrm{i}ka}}{2}\left(a_0^{(s)} - a_0^{(a)}\right). \tag{24b}$$

3.2 Solution for three-dimensional model

For circular geometry, the potential can be expressed in terms of cylindrical polar coordinates (r,θ,z), as (Peter et al., 2004)

$$\phi(r,\theta,z) = \mathrm{e}^{k_0 x}\phi_0(z) + \sum_{n=-N}^{N}\sum_{m=0}^{M} a_{mn}K_n(k_m r)\mathrm{e}^{\mathrm{i}n\theta}\phi_m(z), \quad r > a, \tag{25}$$

and

$$\phi(r,\theta,z) = \sum_{n=-N}^{N}\sum_{m=-2}^{M} b_{mn}I_n(\kappa_m r)\mathrm{e}^{\mathrm{i}n\theta}\psi_m(z), \quad r < a, \tag{26}$$

for suitably large N and M, where I_n and K_n are modified Bessel functions, a_{mn} and b_{mn} are the coefficients of the potential in the open water and the plate covered region, respectively. We note that

$$\phi_I(\mathbf{x},z) = \sum_{n=-N}^{N} I_n(k_0 r)\phi_0(z)\,\mathrm{e}^{\mathrm{i}n\theta}. \tag{27}$$

As in the solution method for the two-dimensional problems, we use the continuity of potential and its horizontal derivative (radial in this case) across the interface between open and ice-covered water, $r = a$. Using orthogonality of the angular (Fourier) modes, we have

$$I_n(k_0 a)\phi_0(z) + \sum_{m=0}^{M} a_{mn}K_n(k_m a)\phi_m(z) = \sum_{m=-2}^{\infty} b_{mn}I_n(\kappa_m a)\psi_m(z) \tag{28}$$

and

$$k_0 I_n'(k_0 a)\phi_0(z) + \sum_{m=0}^{M} a_{mn}k_m K_n'(k_m a)\phi_m(z) = \sum_{m=-2}^{\infty} b_{mn}\kappa_m I_n'(\kappa_m a)\psi_m(z) \tag{29}$$

for $n = -N, \ldots, N$. Multiplying each equations by $\phi_l(z)$ $(l = 0, \ldots, M)$ and integrating over $z \in (-H, 0)$, from $-H$ to 0, gives the system

$$I_n(k_0 a) A_0 \delta_{0l} + a_{ln} K_n(k_l a) A_l = \sum_{m=-2}^{\infty} b_{mn} I_n(\kappa_m a) B_{ml} \tag{30}$$

$$k_0 I_n'(k_0 a) A_0 \delta_{0l} + a_{ln} k_l K_n'(k_l a) A_l = \sum_{m=-2}^{\infty} b_{mn} \kappa_m I_n'(\kappa_m a) B_{ml} \tag{31}$$

for $l = 0, 1, \ldots, M$ and $n = -N, \ldots, N$. Equation (30) can be solved for the open water coefficients, such that

$$a_{ln} = -\frac{I_n(k_0 a)}{K_n(k_0 a)} \delta_{0l} + \sum_{m=-2}^{\infty} b_{mn} \frac{I_n(\kappa_m a) B_{ml}}{K_n(k_l a) A_l}, \tag{32}$$

for $l = 0, 1, \ldots, M$ and $n = -N, \ldots, N$, which can then be substituted into equation (31) to give

$$\begin{aligned} &\left(k_0 I_n'(k_0 a) - k_0 \frac{K_n'(k_0 a)}{K_n(k_0 a)} I_n(k_0 a) \right) A_0 \delta_{0l} \\ &\quad = \sum_{m=-2}^{\infty} \left(\kappa_m I_n'(\kappa_m a) - k_l \frac{K_n'(k_l a)}{K_n(k_l a)} I_n(\kappa_m a) \right) B_{ml} b_{mn} \end{aligned} \tag{33}$$

for $l = 0, 1, \ldots, M$ and $n = -N, \ldots, N$.

Free-edge conditions (3g–h) become

$$\sum_{m=-2}^{\infty} \hat{b}_{mn} \left(\kappa_m^2 I_n(\kappa_m a) - \frac{1-\nu}{a} \left(\kappa_m I_n'(\kappa_m a) - \frac{n^2}{a} I_n(\kappa_m a) \right) \right) = 0, \tag{34a}$$

$$\sum_{m=-2}^{\infty} \hat{b}_{mn} \left(\kappa_m^3 I_n'(\kappa_m a) + n^2 \frac{1-\nu}{a^2} \left(\kappa_m I_n'(\kappa_m a) + \frac{1}{a} I_n(\kappa_m a) \right) \right) = 0, \tag{34b}$$

for $n = -N, \ldots, N$, where $\hat{b}_{mn} = b_{mn} / (F\kappa_m^4 + 1 - K\gamma)$. Combined with equation (33), these conditions give the required equations to solve for the coefficients of the water velocity potential in the plate covered region. The systems are solved for the different angular modes $n = 0, 1, \ldots, N$ separately, noting that the amplitudes for negative values of n are complex conjugates of their positive n counterparts.

The propagating part of the scattered wave is

$$\phi_0(z) = \sum_{n=-N}^{N} a_{0n} K_n(k_0 r) \mathrm{e}^{\mathrm{i}n\theta} \sim \phi_0(z) r^{-1/2} D(\theta - \theta') e^{\mathrm{i}kr} \quad \text{for large } r, \tag{35}$$

where

$$D(\theta) = \mathrm{i} \sqrt{\frac{\pi}{2k}} \sum_{n=-N}^{N} a_{0n} \mathrm{e}^{\mathrm{i}n\theta} \tag{36}$$

is the far-field amplitude (where $k = \mathrm{i}k_0$ is the incident wavenumber).

4 Wave energy transport in the MIZ

We derive here a simple way to connect the scattering by a single floe with attenuation for a large number of floes. We begin with a simplified model for wave energy transport in the MIZ, using the model which only considers the terms due to ice

$$(\partial_t + \mathbf{c}_g \cdot \nabla)\, N(\mathbf{x}, t, \theta) = S_{ice}. \tag{37}$$

Equation (37) is solved for the wave action density $N(\mathbf{x}, t, \theta)$, where θ denotes wave direction. On the left-hand side of (37), $\mathbf{c}_g$ is the group velocity, and $\nabla = (\partial_x, \partial_y)$ is the gradient operator. The term on the right-hand side, S_{ice}, is the source term for wave–ice interactions, which, similar to Dumont et al. (2011) and Williams et al. (2013a,b), we express as

$$S_{ice} = -c_g a_{ice} \alpha N(\mathbf{x}, t, \theta) \quad \text{where} \quad c_g = |\mathbf{c}_g|, \tag{38}$$

a_{ice} is the areal concentration of the ice cover, and α is the attenuation coefficient. For simplicity, the chosen form of S_{ice} neglects nonlinear dissipative phenomena, believed to occur during wave–ice interactions in the scattering regime, particularly overwash (Skene et al., 2015; Nelli et al., 2020), and floe–floe collisions (Shen and Squire, 1998; Bennetts and Williams, 2015; Yiew et al., 2017).

4.1 Attenuation coefficient for two-dimensional scattering

For the two-dimensional scattering model, the attenuation coefficient is expressed as $\alpha = \hat{\alpha}/(2a)$, where $\hat{\alpha}$ is the attenuation per floe, which is

$$\hat{\alpha} = -\log(|\mathcal{T}|^2), \tag{39}$$

where $|\mathcal{T}|^2$ represents the energy transmitted by an individual floe. The attenuation coefficient (39) is based on the assumption that all reflected energy is removed from the wave field, which is equivalent to incoherent wave interactions between the floes. This formula is based on results from scattering theory, which show how the scattering from a large number of randomly spaced scatterers is connected with individual scattering. Details of this derivation can be found in (Bennetts and Squire, 2012). This formula only works in two–dimensions. Resonance occurs for certain combinations of wave period and floe length, such that $|T| \approx 1$, and this leads to unrealistic values of the attenuation coefficient, $\hat{\alpha} = 0$ (Williams et al., 2013a). Therefore, it is typical to average the transmitted energy over a distribution of floe lengths, so that

$$\hat{\alpha} = -\log(\langle |\mathcal{T}|^2 \rangle), \tag{40}$$

where $\langle \cdot \rangle$ denotes average, which is chosen to be normally distributed with a standard deviation $2a/5$. The choice of standard deviation is somewhat arbitrary, but the results presented in §5 are largely insensitive to the variations in the standard deviation.

4.2 Attenuation coefficient for three-dimensional scattering

For the three-dimensional scattering model, we propose the attenuation coefficient is

$$\alpha = \frac{1}{A_f} \int_0^{2\pi} |D(\theta)|^2 \, \mathrm{d}\theta, \tag{41}$$

where $A_f = \pi a^2$ is the area of the ocean surface occupied by an individual floe, and the integral is proportional to the energy scattered by the floe (Meylan et al., 1997). Attenuation coefficient (41) is based on the assumption that all scattered energy is removed from the wave field. This is an approximation that sets an upper bound on the effect of scattering. More complicated scattering models are possible (Meylan et al., 2020).

4.3 Floe Size Distribution

To keep the model simple and easy to implement (and evaluate), the results we present here, and the accompanying code, assume all floes are the same size. It would be possible to extend the model to a distribution of floe sizes by a suitably weighted average of the results calculated here. This would, of course, also depend on having a suitable floe size distribution. This is different from the averaging used in the two-dimensional calculations where the floe size distribution was assumed to be normal.

5 Results

5.1 Comparison of two- and three-dimensional attenuation coefficients

We present a few representative figures for the attenuation coefficient, comparing the two and three-dimensional scattering models. We choose the water depth to be the wavelength of the open water wave to approximate infinite depth and set $M = N = 10$ in the expansion formulae. Figure 1 shows the attenuation coefficient as a function of wave period for thickness $h = 0.5\,\mathrm{m}$, and for floe radius $a = 5\,\mathrm{m}$, $10\,\mathrm{m}$, $25\,\mathrm{m}$ and $50\,\mathrm{m}$.

The sharp drops in the attenuation coefficient at certain periods for the two-dimensional case without averaging is caused by resonance. More resonances occur as the floe length increases. The resonance is caused by constructive interference of waves reflected at the ends of the ice floe, analogous to a Fabry—Perot interferometer. It occurs because waves propagate through the flexible ice floe. This is a two-dimensional phenomenon and does not occur for the three-dimensional model in the same simple manner (since waves are not restricted to travelling in only the forward and backward direction. The resonances are primarily eliminated by averaging, although inflexions in the attenuation coefficient still occur at the resonant periods. We average by sampling with the mean floe length specified and with a standard deviation one–tenth the mean floe length for our calculations here. There is some evidence of weak resonance for the three-dimensional case, with inflexions for the two largest radii. The averaging over angle also helps to reduce resonant effects in the three–dimensional case. Note that the resonance occurs at multiples of the wavelength to floe length. As the floes become larger, there is more possibility for resonances for the wave periods we consider. There is no simple formula for these resonances because the wavelength under the ice changes from that of open water, and there is no simple value for the reflection.

Figures 2, 3, and 4 show similar results for floe thickness $h = 1\,\mathrm{m}$, $1.5\,\mathrm{m}$, and $2\,\mathrm{m}$, respectively. Away from resonances, the attenuation coefficient for the two-dimensional model is higher than the attenuation coefficient for the three-dimensional model for relatively long periods, i.e. periods corresponding to wavelengths much greater than the floe radius. The difference is up to two orders of magnitude for long periods and the smallest floes, $a = 5\,\mathrm{m}$. More typically, the two- and three-dimensional scattering models give attenuation coefficients of the same order of magnitude, and the three-dimensional case often exceeds the two-dimensional case for the larger floe radii. From now on, results for the three-dimensional case only will be considered.

5.2 Power laws

Figure 5 shows log–log plots of the attenuation coefficient, as a function of wave period for different ice thicknesses. For relatively long periods (wavelengths greater than the floe radius), the attenuation coefficient versus wave period is a straight line with a negative slope in log–log space. Therefore, in the long-period regime, the attenuation coefficient obeys a power law of the form

$$\alpha \propto T^{-p}, \tag{42}$$

and the best-fit values of p for the different thicknesses are shown in the legends. The value of p is ≥ 8, which is much greater than the values obtained from field measurements, i.e. $p \approx 2$ (Meylan

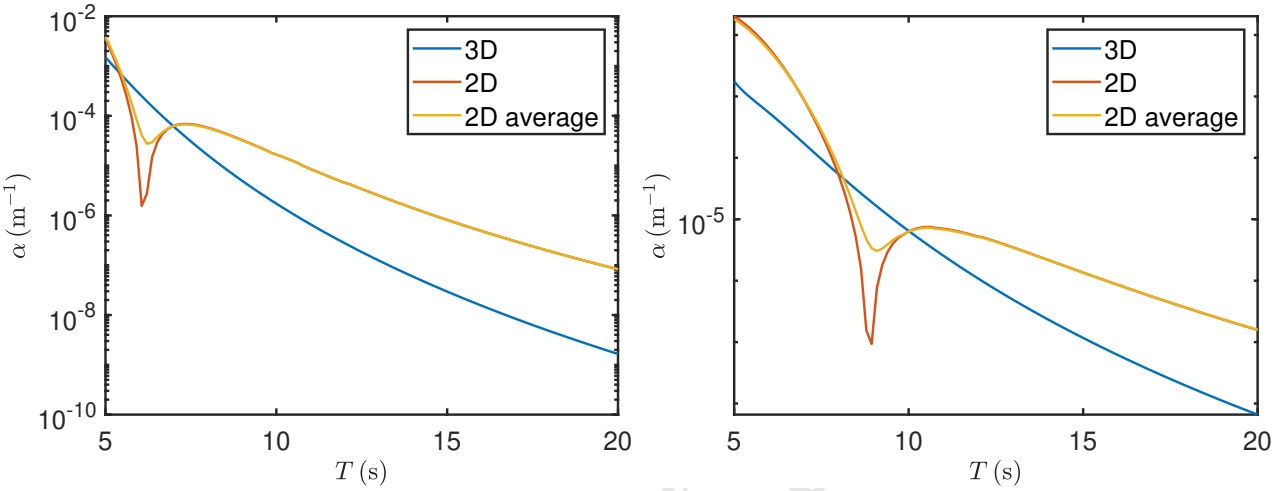

(a) Radius or mean radius $a = 5\,\mathrm{m}$

(b) Radius or mean radius $a = 10\,\mathrm{m}$

(c) Radius or mean radius $a = 25\,\mathrm{m}$

(d) Radius or mean radius $a = 50\,\mathrm{m}$

Figure 1: Attenuation α versus period T for the two and three dimensional methods for floe thickness $h = 0.5\,\mathrm{m}$.

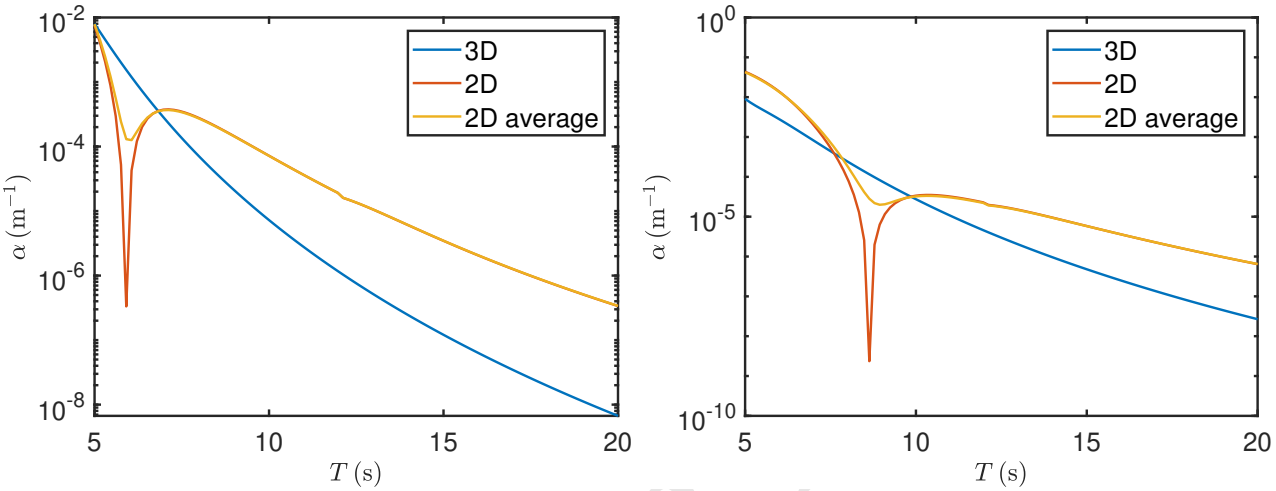

(a) Radius or mean radius $a = 5\,\mathrm{m}$

(b) Radius or mean radius $a = 10\,\mathrm{m}$

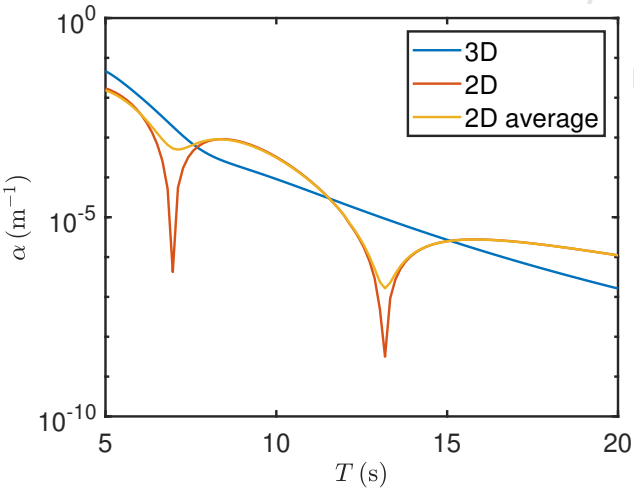

(c) Radius or mean radius $a = 25\,\mathrm{m}$

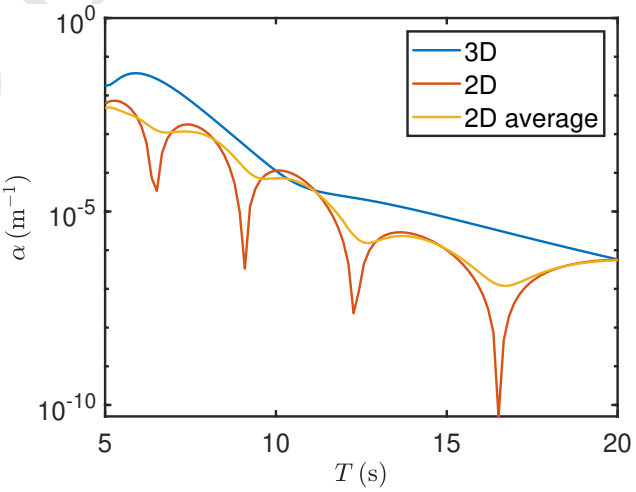

(d) Radius or mean radius $a = 50\,\mathrm{m}$

Figure 2: As in Figure 1 except the floe thickness is $h = 1\,\mathrm{m}$.

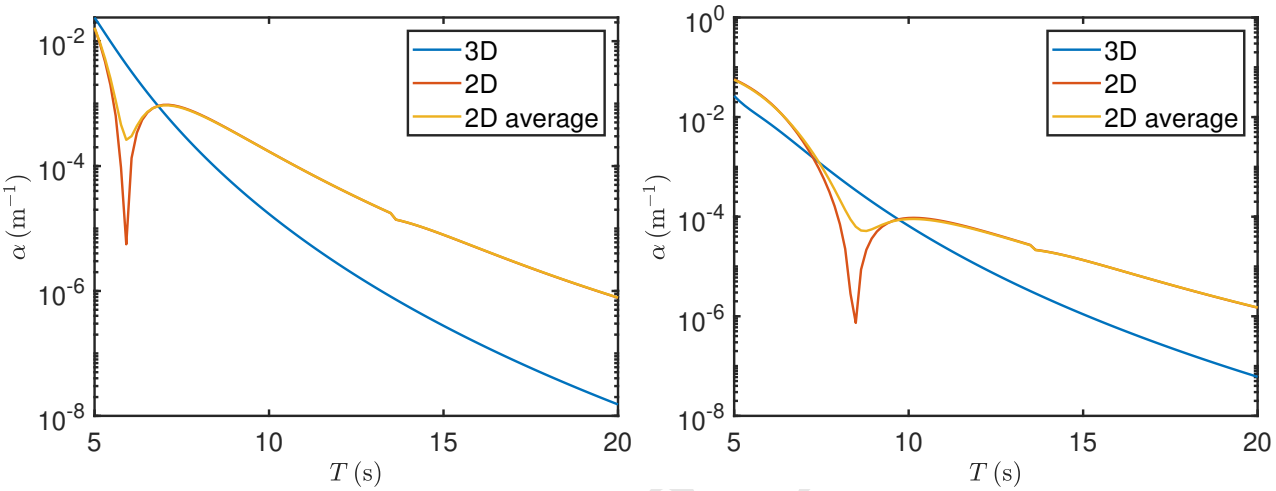

(a) Radius or mean radius $a = 5\,\mathrm{m}$

(b) Radius or mean radius $a = 10\,\mathrm{m}$

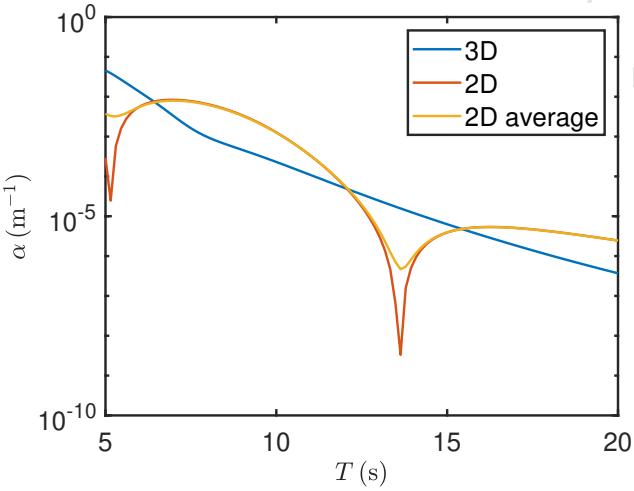

(c) Radius or mean radius $a = 25\,\mathrm{m}$

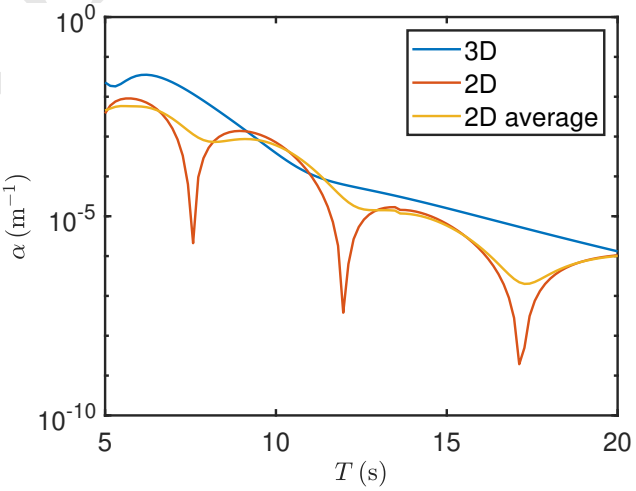

(d) Radius or mean radius $a = 50\,\mathrm{m}$

Figure 3: As in Figure 1 except the floe thickness is $h = 1.5\,\mathrm{m}$.

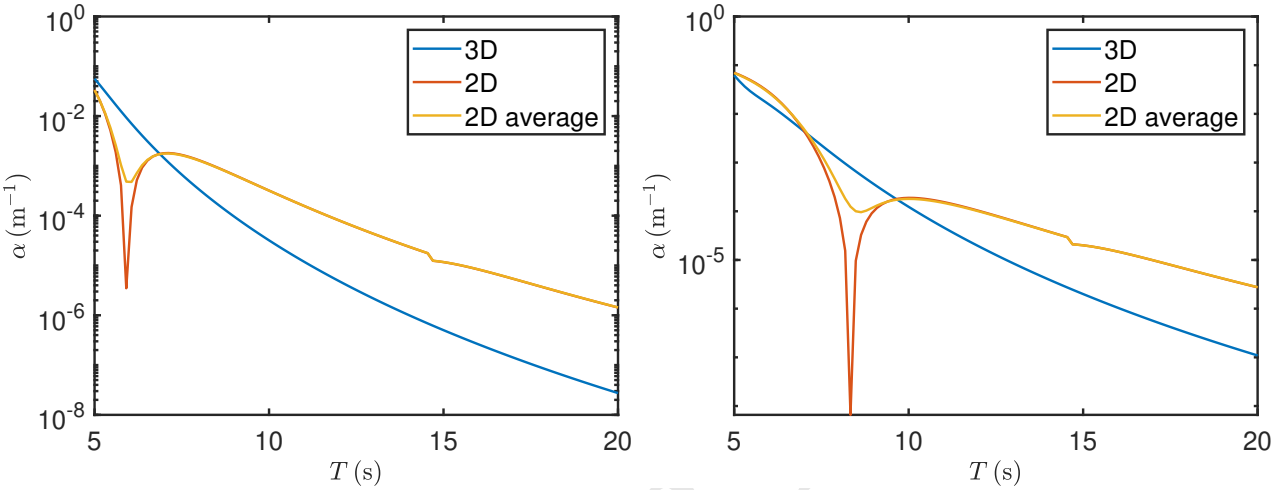

(a) Radius or mean radius $a = 5\,\mathrm{m}$

(b) Radius or mean radius $a = 10\,\mathrm{m}$

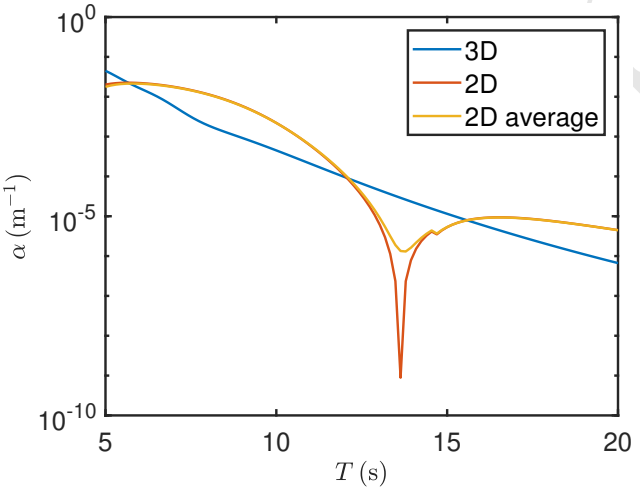

(c) Radius or mean radius $a = 25\,\mathrm{m}$

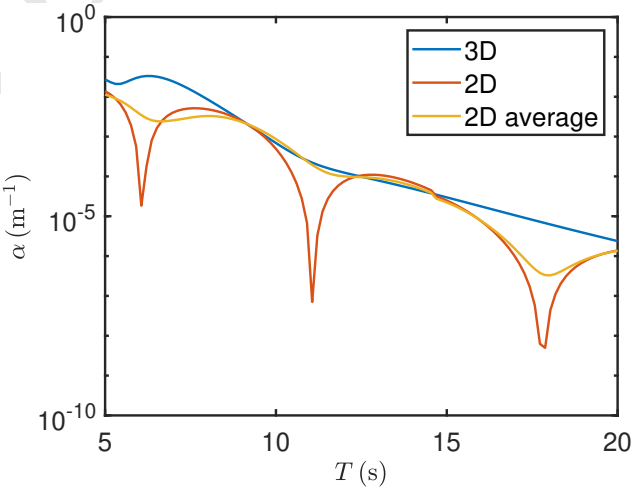

(d) Radius or mean radius $a = 50\,\mathrm{m}$

Figure 4: As in Figure 1 except the floe thickness is $h = 2\,\mathrm{m}$.

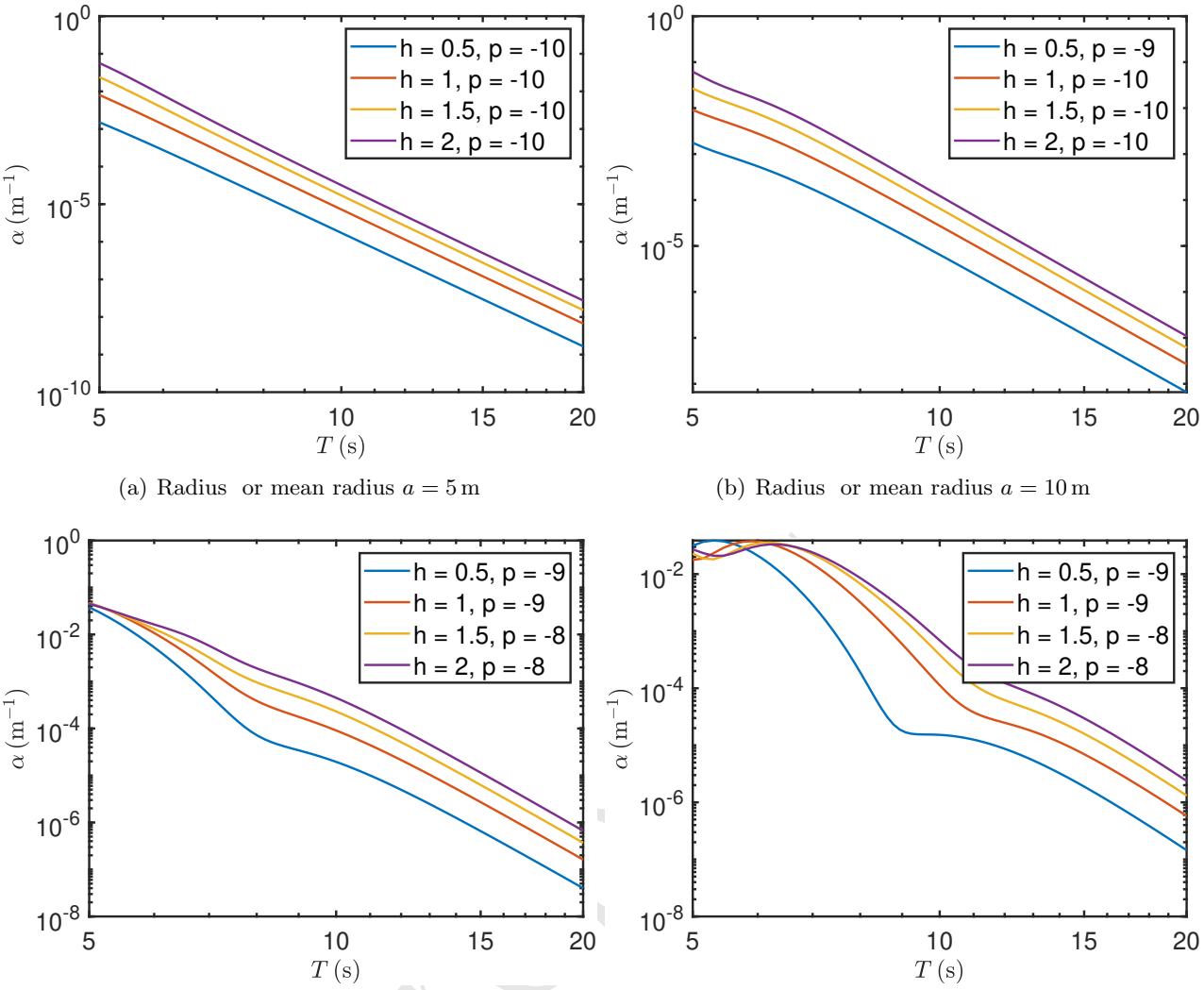

(a) Radius or mean radius $a = 5\,\mathrm{m}$

(b) Radius or mean radius $a = 10\,\mathrm{m}$

(c) Radius or mean radius $a = 25\,\mathrm{m}$

(d) Radius or mean radius $a = 50\,\mathrm{m}$

Figure 5: A log–log plot of the attenuation α as a function of period T for the thicknesses shown. The coefficient T is a linear fit in log-log space to give power law relationship in equation (42).

et al., 2014) or 3 (Thomson et al., 2021).

Figure 6 shows log–log plots of the attenuation coefficient as a function of ice thickness, for different values of wave period and floe radius. For relatively long periods, the attenuation is a straight line with positive slope, and therefore

$$\alpha \propto h^q \quad \text{for} \quad T \quad \text{large.} \tag{43}$$

The legends show the best-fit values of q, from which we observe that q is generally insensitive to the wave period and floe radius, and $q \approx 2$. The complicated curves for small floes seen in Figure 6 (a) are caused by resonance effect for rigid floes at short periods, such as a resonant bobbing motion.

5.3 Extending the model to heterogeneous distributions of floes.

A single floe size cannot describe ice floes in the MIZ. It would be possible to extend the model to the case of floe size distributions by averaging the effects of each floe size. We do not attempt that here but note that this would be the logical next step if the scattering model is proven to be suitable.

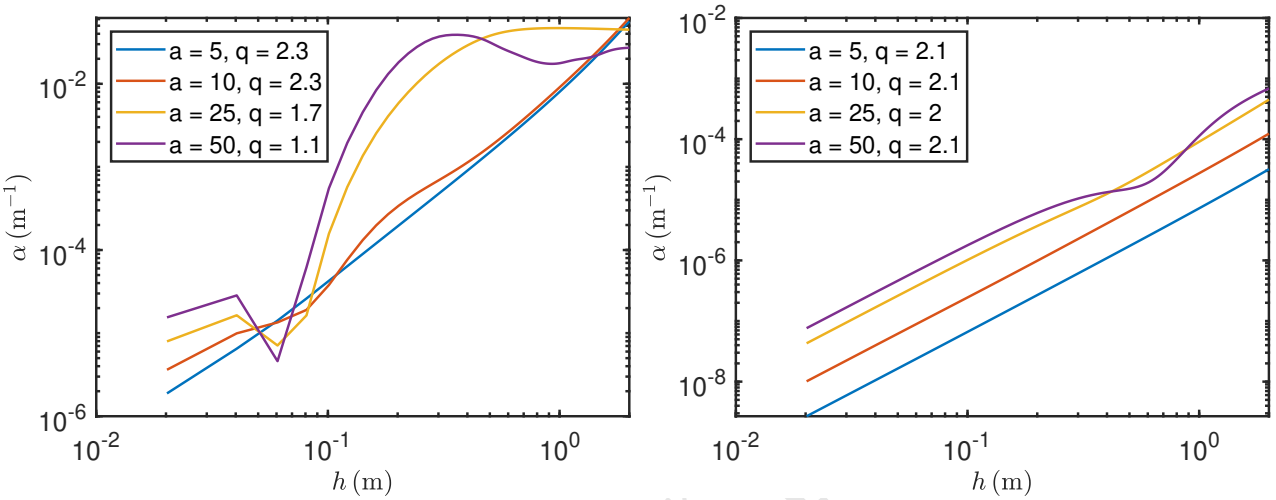

(a) Period $T = 5\,\mathrm{s}$

(b) Period $T = 10\,\mathrm{s}$

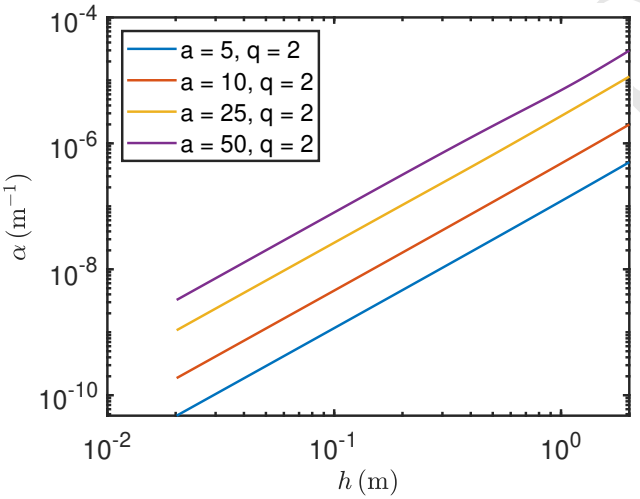

(c) Period $T = 15\,\mathrm{s}$

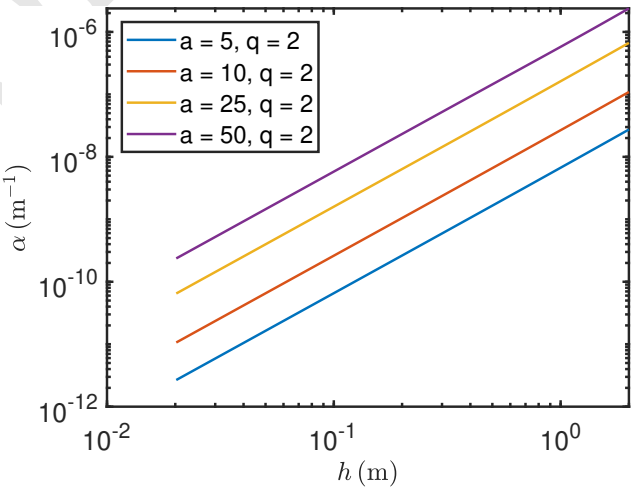

(d) Period $T = 20\,\mathrm{s}$

Figure 6: Log–log plot of attenuation coefficient α as a function of ice thickness h. The coefficient q is a linear fit in log-log space to give power law relationship in equation (43)

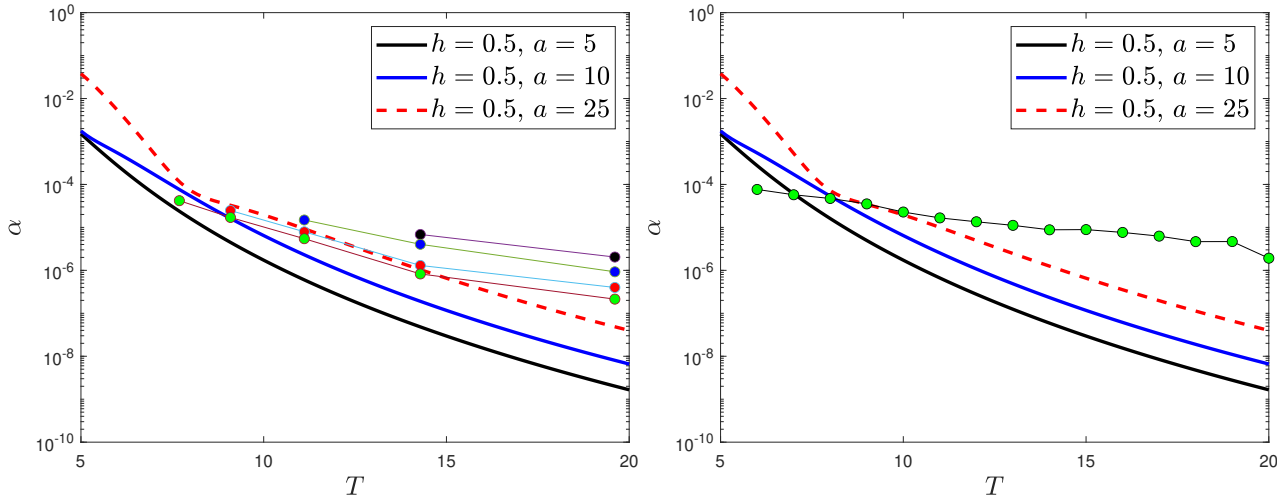

(a) Variation of a

(b) Variation of h

Figure 7: Comparison of attenuation coefficient α from the three-dimensional scattering model (solid thick lines) with measured attenuation (lines with dots). In (a) the results are from Rogers et al. (2020). The four curves are a sorting based on noise sensitivity. In (b) the comparison is with the measurements of Meylan et al. (2014) with an updated analysis correctly accounting for noise floor (Thomson et al., 2021).

6 Comparison with experiments results

Figure 7 shows a comparison of the attenuation coefficient given by the three-dimensional scattering model, with attenuation coefficient (44), as given by Meylan et al. (2014). Attenuation due to scattering dominates for short periods, and the empirical attenuation coefficient dominates for long periods. In field measurements, only long-period attenuation is likely observed because the scattering attenuation has removed the short periods over a short distance close to the ice edge.

Figure 7 shows a comparison of the attenuation coefficient given by the three-dimensional scattering model, with experimental data. Figures 7 (a) shows a comparison with the analysis presented in Rogers et al. (2020) in which the fitting is based on wave prediction computational code. We believe this is likely the most accurate experimental results. The four different lines were based on the sorting of the profiles by their length used in Rogers et al. (2020). The length is closely related to the wave intensity as a noise floor cut off was used. We also note that the negative results were discarded so that a possible upward bias was introduced into the mean values for the low–intensity cases. The estimated values for the ice thickness was 0.51 m, 0.50 m, 047 m, and 0.37 m for the shortest to longest respectively. We run the comparison with a thickness of 0.5m and a radius of 5m, 10m, and 25m (assuming concentration is 100%). The agreement with the 25m radius and the longest results is remarkable. However, we do not claim that this is sufficient comparison to validate our model or conclusively prove it. We also note that there is a clear divergence in the attenuation for long periods.

Figures 7 (b) shows a comparison with the results first presented in Meylan et al. (2014) but updated with a recent analysis which takes into account the noise floor of the wave buoys (Thomson et al., 2021). In this case, the comparison is nowhere near as good and the clear problem for long periods is apparent. We note that there is no tuning in these results.

7 Long-period dissipation

It is clear from the comparison with measurements that scattering cannot account for the dissipation at long periods. We propose that the attenuation due to scattering be augmented by the empirical

model

$$\alpha = c_1 T^{-2} + c_2 T^{-4}, \tag{44}$$

where $c_1 = 2.12 \times 10^{-3}$ (s^2/m) and $c_2 = 4.59 \times 10^{-2}$ (s^4/m), which is based on measurements reported by Meylan et al. (2014). Note that the coefficients c_1 and c_2 are likely to depend on the ice conditions, but the dependencies have not yet been resolved by measurements or theory. Note also that the evidence for the second T^{-4} term is not as strong as for the first T^{-2} term. We also note that recent evidence (Rogers et al., 2020; Thomson et al., 2021) suggest that T^{-3} may be more appropriate. We also note the numerical study of Guyenne and Parau (2017) which supports the idea that for short waves scattering dominates while for long waves it is viscous damping which dominates.

8 Summary and discussion

Attenuation of waves due to scattering by ice floes has been investigated. A comparison of the two- and three-dimensional models showed that the models generally agree in the regime where scattering dominates, notwithstanding resonances that occur primarily on the two-dimensional model. In general, it was shown that the three-dimensional model eliminates does not require need for averaging to eliminate resonances, as in the two-dimensional model. The long-period asymptotic behaviour of the attenuation coefficient for the three-dimensional scattering model was shown to be approximately T^{-8}, i.e. attenuation due to scattering dies out quickly as period increases. It was deduced that scattering could not account for observed long-period attenuation, where the exponent has been ≈ 2. We believe this is due to a viscous damping type model or similar, but note that no model or physical process has been found which reproduces this behaviour. We, therefore, propose that the scattering model include an additional parameterised scattering term based on measurements. We have provided the computer code as supplementary material, and we anticipate that further developments can be made to it as our understanding advances. We hypothesise that the scattering model will be necessary during breakup events when the ice cover transitions from quasi-continuous to a field of relatively small floes. At this point, the long-period dissipation model will prevail. We note that the key parameters required for models are the floe thickness and floe size distributions. Both of these are difficult to measure over large areas of the MIZ

Acknowledgements

The authors thank the Isaac Newton Institute for Mathematical Sciences for support and hospitality during the programme Mathematics of Sea Ice Phenomena (EPSRC grant number EP/K032208/1), when work on this paper was undertaken, and during which MHM and LGB were supported by grants from the Simons Foundation. This work is funded by the Australian Research Council (DP200102828). LGB is supported by an Australian Research Council midcareer fellowship (FT190100404). CH thanks the National Institute of Water and Atmospheric Science in New Zealand for their hospitality and acknowledges support from the Voss Postdoctoral Fellowship at Brown University and NASA Grant GR5227091.

References

Alberello, A., Bennetts, L., Heil, P., Eayrs, C., Vichi, M., MacHutchon, K., Onorato, M., Toffoli, A., 2020. Drift of pancake ice floes in the winter antarctic marginal ice zone during polar cyclones. Journal of Geophysical Research: Oceans 125 (3), e2019JC015418.

Ardhuin, F., Otero, M., Merrifield, S., Grouazel, A., Terrill, E., 2020. Ice breakup controls dissipation of wind waves across southern ocean sea ice. Geophys. Res. Lett. 47 (13), e2020GL087699.

Ardhuin, F., Sutherland, P., Doble, M., Wadhams, P., 2016. Ocean waves across the Arctic: Attenuation due to dissipation dominates over scattering for periods longer than 19 s. Geophysical Research Letters 43 (11), 5775–5783.

Bateson, A. W., Feltham, D. L., Schröder, D., Hosekova, L., Ridley, J. K., Aksenov, Y., 2020. Impact of sea ice floe size distribution on seasonal fragmentation and melt of arctic sea ice. Cryosphere 14 (2), 403–428.

Bennetts, L., Alberello, A., Meylan, M., Cavaliere, C., Babanin, A., Toffoli, A., 2015. An idealised experimental model of ocean surface wave transmission by an ice floe. Ocean Model. 96, 85–92.

Bennetts, L., Squire, V., 2009. Wave scattering by multiple rows of circular ice floes. J. Fluid Mech. 639, 213–238.

Bennetts, L., Williams, T., 2010. Wave scattering by ice floes and polynyas of arbitrary shape. Journal of Fluid Mechanics 662, 5–35.

Bennetts, L., Williams, T., 2015. Water wave transmission by an array of floating discs. Proc. R. Soc. A 471 (2173), 20140698.

Bennetts, L. G., Biggs, N. R. T., Porter, D., 2007. A multi–mode approximation to wave scattering by ice sheets of varying thickness. J. Fluid Mech. 579, 413–443.

Bennetts, L. G., O'Farrell, S., Uotila, P., 2017. Impacts of ocean-wave-induced breakup of Antarctic sea ice via thermodynamics in a stand-alone version of the CICE sea-ice model. The Cryosphere 11 (3), 1035–1040.

Bennetts, L. G., Peter, M. A., Squire, V. A., Meylan, M. H., 2010. A three-dimensional model of wave attenuation in the marginal ice zone. J. Geophys. Res. 115.

Bennetts, L. G., Squire, V. A., 2012. On the calculation of an attenuation coefficient for transects of ice-covered ocean. Proc. Roy. Soc. Lon. A 468 (2137), 136–162.

Boutin, G., Ardhuin, F., Dumont, D., Sévigny, C., Girard-Ardhuin, F., Accensi, M., 2018. Floe size effect on wave-ice interactions: Possible effects, implementation in wave model, and evaluation. J. Geophys. Res.-Oceans 123 (7), 4779–4805.

Boutin, G., Lique, C., Ardhuin, F., Rousset, C., Talandier, C., Accensi, M., Girard-Ardhuin, F., 2020. Towards a coupled model to investigate wave–sea ice interactions in the arctic marginal ice zone. Cryosphere 14 (2), 709–735.

Chen, H., Gilbert, R. P., Guyenne, P., 2019a. Dispersion and attenuation in a porous viscoelastic model for gravity waves on an ice-covered ocean. Eur. J. Mech. B-Fluids 78, 88–105.

Chen, Z., Bromirski, P., Gerstoft, P., Stephen, R., Lee, W., Yun, S., Olinger, S., Aster, R., Wiens, D., Nyblade, A. A., 2019b. Ross ice shelf icequakes associated with ocean gravity wave activity. Geophysical Research Letters 46 (15), 8893–8902.

Cheng, S., Rogers, W. E., Thomson, J., Smith, M., Doble, M. J., Wadhams, P., Kohout, A. L., Lund, B., Persson, O. P. G., Collins, C. O., Ackley, S., Montiel, F., Shen, H. H., 2017. Calibrating a viscoelastic sea ice model for wave propagation in the Arctic fall marginal ice zone. J. Geophys. Res., 1–24.

Cheng, S., Stopa, J., Ardhuin, F., Shen, H. H., 2020. Spectral attenuation of ocean waves in pack ice and its application in calibrating viscoelastic wave-in-ice models. Cryosphere 14 (6), 2053–2069.

Collins, C. O., Rogers, W. E., Marchenko, A., Babanin, A. V., 2015. In situ measurements of an energetic wave event in the Arctic marginal ice zone. Geophys. Res. Lett. 42 (6), 1863–1870.

Doble, M. J., De Carolis, G., Meylan, M. H., Bidlot, J.-R., Wadhams, P., 2015. Relating wave attenuation to pancake ice thickness, using field measurements and model results. Geophysical Research Letters 42 (11), 4473–4481.

Dolatshah, A., Nelli, F., Bennetts, L. G., Alberello, A., Meylan, M. H., Monty, J. P., Toffoli, A., 2018. Hydroelastic interactions between water waves and floating freshwater ice. Physics of Fluids 30 (9), 091702.

Dumont, D., Kohout, A. L., Bertino, L., 2011. A wave-based model for the marginal ice zone including a floe breaking parameterization. J. Geophys. Res. 116.

Fox, C., Squire, V. A., 1994. On the oblique reflexion and transmission of ocean waves at shore fast sea ice. Phil. Trans. R. Soc. Lond. A. 347, 185–218.

Guyenne, P., Parau, E. I., 2017. Numerical simulation of solitary-wave scattering and damping in fragmented sea ice. Proc. 27th Intl. Ocean Polar Engng Conference, pp. 373—-380.

Herman, A., Evers, K.-U., Reimer, N., 2018. Floe-size distributions in laboratory ice broken by waves. The Cryosphere 12 (2), 685–699.

Horvat, C., Blanchard-Wrigglesworth, E., Petty, A., 2020. Observing waves in sea ice with icesat-2. Geophys. Res. Lett. 47 (10), e2020GL087629.

Horvat, C., Tziperman, E., nov 2015. A prognostic model of the sea-ice floe size and thickness distribution. Cryosphere 9 (6), 2119–2134.

Horvat, C., Tziperman, E., Campin, J.-M., aug 2016. Interaction of sea ice floe size, ocean eddies, and sea ice melting. Geophys. Res. Lett. 43 (15), 8083–8090.
URL http://doi.wiley.com/10.1002/2016GL069742

Keller, J. B., 1998. Gravity waves on ice-covered water. Journal of Geophysical Research: Oceans 103 (C4), 7663–7669.

Kohout, A. L., Meylan, M. H., 2008. An elastic plate model for wave attenuation and ice floe breaking in the marginal ice zone. J. Geophys. Res. 113 (C9).

Kohout, A. L., Meylan, M. H., 2009. Wave scattering by multiple floating elastic plates with spring or hinged boundary conditions. Mar. Struct. 22, 712–729.

Kohout, A. L., Williams, M. J., Dean, S., Meylan, M. H., 2014. Storm-induced sea ice breakup and the implications for ice extent. Nature 509 (7502), 604–607.

Kohout, A. L., Williams, M. J. M., Toyota, T., Lieser, J., Hutchings, J., sep 2016. In situ observations of wave-induced sea ice breakup. Deep Sea Research Part II: Topical Studies in Oceanography 131, 22–27.
URL http://linkinghub.elsevier.com/retrieve/pii/S096706451500212X

Liu, A. K., Mollo-Christensen, E., 1988. Wave propagation in a solid ice pack. Journal of Physical Oceanography 18 (11), 1702–1712.

Massom, R. A., Scambos, T. A., Bennetts, L. G., Reid, P., Squire, V. A., Stammerjohn, S. E., 2018. Antarctic ice shelf disintegration triggered by sea ice loss and ocean swell. Nature 558, 383–389.

Meylan, M., Bennetts, L., Cavaliere, C., Alberello, A., Toffoli, A., 2015. Experimental and theoretical models of wave-induced flexure of a sea ice floe. Phys. Fluids 27.

Meylan, M. H., 2002. The wave response of ice floes of arbitrary geometry. J. Geophys. Res. 107 (C6).

Meylan, M. H., Bennetts, L., 2018. Three-dimensional time-domain scattering of waves in the marginal ice zone. Philosophical Transactions of the Royal Society A: Mathematical, Physical and Engineering Sciences 376 (2129), 20170334.

Meylan, M. H., Bennetts, L., Mosig, J., Rogers, W., Doble, M., Peter, M. A., 2018. Dispersion relations, power laws, and energy loss for waves in the marginal ice zone. Journal of Geophysical Research: Oceans 123 (5), 3322–3335.

Meylan, M. H., Bennetts, L. G., Kohout, A. L., 2014. In-situ measurements and analysis of ocean waves in the antarctic marginal ice zone. Geophys. Res. Lett. 41 (14), 5046–5051.

Meylan, M. H., Perrie, W., Toulany, B., Hu, Y., Casey, M., 2020. On the three-dimensional scattering of waves by flexible marginal ice floes. J Geophys. Res.-Oceans 125 (2).

Meylan, M. H., Squire, V. A., 1994. The response of ice floes to ocean waves. J. Geophy. Res. 99 (C1), 891–900.

Meylan, M. H., Squire, V. A., Fox, C., 1997. Towards realism in modeling ocean wave behavior in marginal ice zones. J. Geophy. Res. 102 (C10), 22981–22991.

Montiel, F., Bennetts, L. G., Squire, V. A., Bonnefoy, F., Ferrant, P., 2013a. Hydroelastic response of floating elastic discs to regular waves. Part 1. Wave basin experiments. J. Fluid Mech. 723, 604–628.

Montiel, F., Bennetts, L. G., Squire, V. A., Bonnefoy, F., Ferrant, P., 2013b. Hydroelastic response of floating elastic discs to regular waves. Part 2. Modal analysis. J. Fluid Mech. 723, 629–652.

Montiel, F., Squire, V., Bennetts, L., 2016. Attenuation and directional spreading of ocean wave spectra in the marginal ice zone. J. Fluid Mech. 790, 492–522.

Mosig, J. E. M., Montiel, F., Squire, V. A., 2015. Comparison of viscoelastic-type models for ocean wave attenuation in ice-covered seas. Journal of Geophysical Research: Oceans 120 (9), 6072–6090. URL `http://dx.doi.org/10.1002/2015JC010881 http://doi.wiley.com/10.1002/2015JC010881`

Nelli, F., Bennetts, L., Skene, D., Monty, J., Lee, J., Meylan, M., Toffoli, A., 2017. Reflection and transmission of regular water waves by a thin, floating plate. Wave Motion 70, 209–221.

Nelli, F., Bennetts, L. G., Skene, D. M., Toffoli, A., 2020. Water wave transmission and energy dissipation by a floating plate in the presence of overwash. J. Fluid Mech. 889.

Perrie, W., Hu, Y., 1996. Air–ice–ocean momentum exchange. part 1:energy transfer between waves and ice floes. J. of Phys. Ocean. 26, 1705–1720.

Peter, M. A., Meylan, M. H., 2009. Water-wave scattering by vast fields of bodies. SIAM J. Appl. Math. 70 (5), 1567–1586.

Peter, M. A., Meylan, M. H., Chung, H., 2004. Wave scattering by a circular elastic plate in water of finite depth: a closed form solution. Int. J. Offshore Polar 14 (2), 81–85.

Rabault, J., Sutherland, G., Gundersen, O., Jensen, A., Marchenko, A., Breivik, Ø., 2020. An open source, versatile, affordable waves in ice instrument for scientific measurements in the polar regions. Cold Reg. Sci. Techol. 170, 102955.

Roach, L. A., Bitz, C. M., Horvat, C., Dean, S. M., dec 2019. Advances in Modeling Interactions Between Sea Ice and Ocean Surface Waves. Journal of Advances in Modeling Earth Systems 11 (12), 4167–4181.
URL https://onlinelibrary.wiley.com/doi/abs/10.1029/2019MS001836

Roach, L. A., Horvat, C., Dean, S. M., Bitz, C. M., 2018. An emergent sea ice floe size distribution in a global coupled ocean-sea ice model. J. Geophys. Res.-Oceans 123 (6), 4322–4337.

Rogers, E. W., Meylan, M. H., Kohout, A. L., 2020. Estimates of spectral wave attenuation in antarctic sea ice, using model/data inversion. Cold Reg. Sci. and Tech., 103198.

Rogers, W. E., Thomson, J., Shen, H. H., Doble, M. J., Wadhams, P., Cheng, S., 2016. Dissipation of wind waves by pancake and frazil ice in the autumn b eaufort s ea. J. Geophys. Res.-Oceans 121 (11), 7991–8007.

Shen, H. H., Squire, V. A., 1998. Wave Damping in Compact Pancake Ice Fields Due to Interactions Between Pancakes. In: Jeffries, M. O. (Ed.), Antarctic Research Series. American Geophysical Union, Washington, D. C., pp. 325–341.

Skene, D., Bennetts, L., Meylan, M., Toffoli, A., 2015. Modelling water wave overwash of a thin floating plate. Journal of Fluid Mechanics 777, R3.

Squire, V., Moore, S. C., 1980. Direct measurement of the attentuation of ocean waves by pack ice. Nature 283 (5745), 365 – 368.

Squire, V. A., 2020. Ocean wave interactions with sea ice: a reappraisal. Annu. Rev. Fluid Mech. 52, 37–60.

Sree, D. K. K., Law, A. W.-K., Shen, H. H., 2017. An experimental study on the interactions between surface waves and floating viscoelastic covers. Wave Motion 70, 195–208.

Sutherland, G., Rabault, J., Christensen, K. H., Jensen, A., 2019. A two layer model for wave dissipation in sea ice. Appl. Ocean Res. 88, 111–118.

Sutherland, P., Brozena, J., Rogers, W. E., Doble, M., Wadhams, P., 2018. Airborne remote sensing of wave propagation in the marginal ice zone. J. Geophys. Res.-Oceans 123 (6), 4132–4152.

Thomson, J., Ackley, S., Girard-Ardhuin, F., Ardhuin, F., Babanin, A., Boutin, G., Brozena, J., Cheng, S., Collins, C., Doble, M., et al., 2018. Overview of the arctic sea state and boundary layer physics program. J Geophys. Res.-Oceans 123 (12), 8674–8687.

Thomson, J., Hosekova, L., Meylan, M. H., Kohout, A. L., Kumar, N., 2021. Spurious rollover of wave attenuation rates in sea ice caused by noise in field measurements. J Geophys. Res.-Oceans.

Timco, G., Weeks, W., 2010. A review of the engineering properties of sea ice. Cold Reg. Sci. Techol. 60 (2), 107–129.

Toffoli, A., Bennetts, L. G., Meylan, M. H., Cavaliere, C., Alberello, A., Elsnab, J., Monty, J. P., 2015. Sea ice floes dissipate the energy of steep ocean waves. Geophys. Res. Lett. 42 (20), 8547–8554.

Voermans, J., Babanin, A., Thomson, J., Smith, M., Shen, H., 2019. Wave attenuation by sea ice turbulence. Geophys. Res. Lett. 46 (12), 6796–6803.

Wadhams, P., Squire, V. A., Goodman, D. J., Cowan, A. M., Moore, S. C., 1988. The attenuation rates of ocean waves in the marginal ice zone. J. Geophys. Res. 93 (C6), 6799 – 6818.

Wang, R., Shen, H. H., 2010a. Gravity waves propagating into an ice-covered ocean: A viscoelastic model. Journal of Geophysical Research 115 (C6), C06024.
URL http://dx.doi.org/10.1029/2009JC005591 http://doi.wiley.com/10.1029/2009JC005591

Wang, R., Shen, H. H., 2010b. Gravity waves propagating into an ice-covered ocean: A viscoelastic model. J. Geophys. Res. 115 (C6).

Weber, J. E., 1987. Wave attenuation and wave drift in the marginal ice zone. J. Phys. Oceanogr. 17 (12), 2351–2361.

Williams, T. D., Bennetts, L. G., Squire, V. A., Dumont, D., Bertino, L., 2013a. Wave–ice interactions in the marginal ice zone. Part 1: Theoretical foundations. Ocean Model. 71, 81–91.

Williams, T. D., Bennetts, L. G., Squire, V. A., Dumont, D., Bertino, L., 2013b. Wave–ice interactions in the marginal ice zone. Part 2: Numerical implementation and sensitivity studies along 1D transects of the ocean surface. Ocean Model. 71, 92–101.

Williams, T. D., Rampal, P., Bouillon, S., 2017. Wave–ice interactions in the neXtSIM sea-ice model. The Cryosphere 11 (5), 2117–2135.

Yiew, L. J., Bennetts, L. G., Meylan, M. H., French, B. J., Thomas, G. A., 2016. Hydrodynamic responses of a thin floating disk to regular waves. Ocean Model. 97, 52–64.

Yiew, L. J., Bennetts, L. G., Meylan, M. H., Thomas, G. A., French, B. J., 2017. Wave-induced collisions of thin floating disks. Physics of Fluids 29 (12), 127102.

Zhang, J., Stern, H., Hwang, B., Schweiger, A., Steele, M., Stark, M., Graber, H. C., 2016. Modeling the seasonal evolution of the Arctic sea ice floe size distribution. Elem Sci Anth 4, 000126.